Swimmers Heal on the Move Following Catastrophic Damage

Emil Karshalev,[§] Cristian Silva-Lopez,[§] Kyle Chan, Jieming Yan, Elodie Sandraz, Mathieu Gallot, Amir Nourhani, Javier Garay, and Joseph Wang*

Cite This: *Nano Lett.* 2021, 21, 2240−2247

Read Online

ACCESS | Metrics & More | Article Recommendations | Supporting Information

ABSTRACT: Herein, we describe the development of 2D self-healing small-scale swimmers capable of autonomous propulsion and "on-the-fly" structural recovery in large containers. Incorporation of magnetic $Nd_2Fe_{14}B$ microparticles in specialized printed strips results in rapid reorientation and reattachment of the moving tail to its complementary broken static piece to restore the original swimmer structure and propulsion behavior. The swimmers display functional recovery independent of user input. Measurements of the magnetic hysteresis and fields were used to assess the behavior of the healing mechanism in real swimming situations. Damage position and multiple magnetic strip patterns have been examined and their influence upon the recovery efficiency has been compared. Owing to its versatility, fast response, and simplicity the new self-healing strategy represents an important step toward the development of new "on-the-fly" repairing strategies for small-scale swimmers and robots.

KEYWORDS: *self-healing, magnetic interactions, layered structure, self-propelled, autonomous motion*
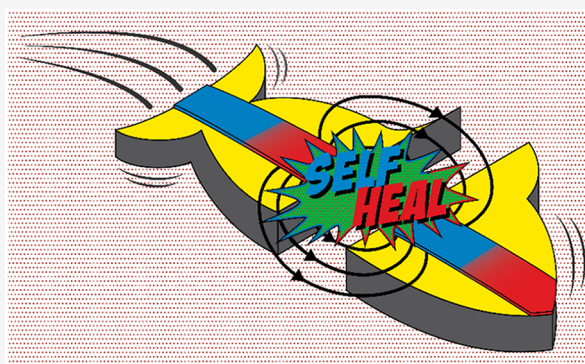
Self-healing is an essential property of living organisms and a major challenge for artificial systems; thus, the development of effective repair strategies is of tremendous interest. Recently, small- and microscale robots have been developed toward a broad range of applications, ranging from environmental and security remediation, sensing or biomedical drug-delivery, and surgery.[1−8] It is envisioned that these tiny machines are released into harsh environments where multiple hazards can lead to structural damage, resulting in catastrophic failure and cessation of the motion and operation. Traditional rigid, metal-based robots are composed of an array of replaceable parts and do not suffer the limitations of softer polymeric or hydrogel actuators. The latter are vulnerable to damage because of low tear strength and propensity for crack growth.[9−12] Optimal self-healing strategies require recombination to occur autonomously without user input or additional external triggers, which is in contradiction with traditional temperature or light-based chemical healing approaches. Additionally, damage can occur in the same place more than once, requiring healing strategies for such repetitive damage under the dynamically changing conditions encountered with motile robots.

One current self-healing strategy features a soft electronic skin that can sustain large mechanical deformation due to the formation of liquid metal frameworks within a silicone elastomer, but once the material is damaged and depleted, there is no way to recombine it.[13] More closely resembling an appendage, Acome et al. designed hydraulically amplified self-healing electrostatic (HASEL) actuators which can easily regain their actuation performance even after 50 dielectric breakdown cycles.[14] The dielectric prevents permanent damage through dielectric breakdown but comes at the price of diminished performance. Another self-healing strategy utilizes a robotic gripper based on the thermoreversible Diels−Alder reaction to close cracks and punctures; yet, it is not autonomous and requires the application of an external stimulus (temperature) over extended periods (minutes to days).[9,10] Smaller scale robotic systems utilized magnetic interactions to assemble robots into various shapes with a high degree of control.[15−17] However, these strategies require extensive human involvement, with continuous manipulation of multiple magnetic coils and fluidic channel flows, are not explicitly for self-healing, and are only concerned with assembly on very small length scales. Strategies involving chemical bonding and capsule-based systems are easily affected by ambient conditions, limiting the healing behavior in a single site and making them not suitable for healing in harsh environments.[18]
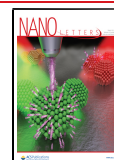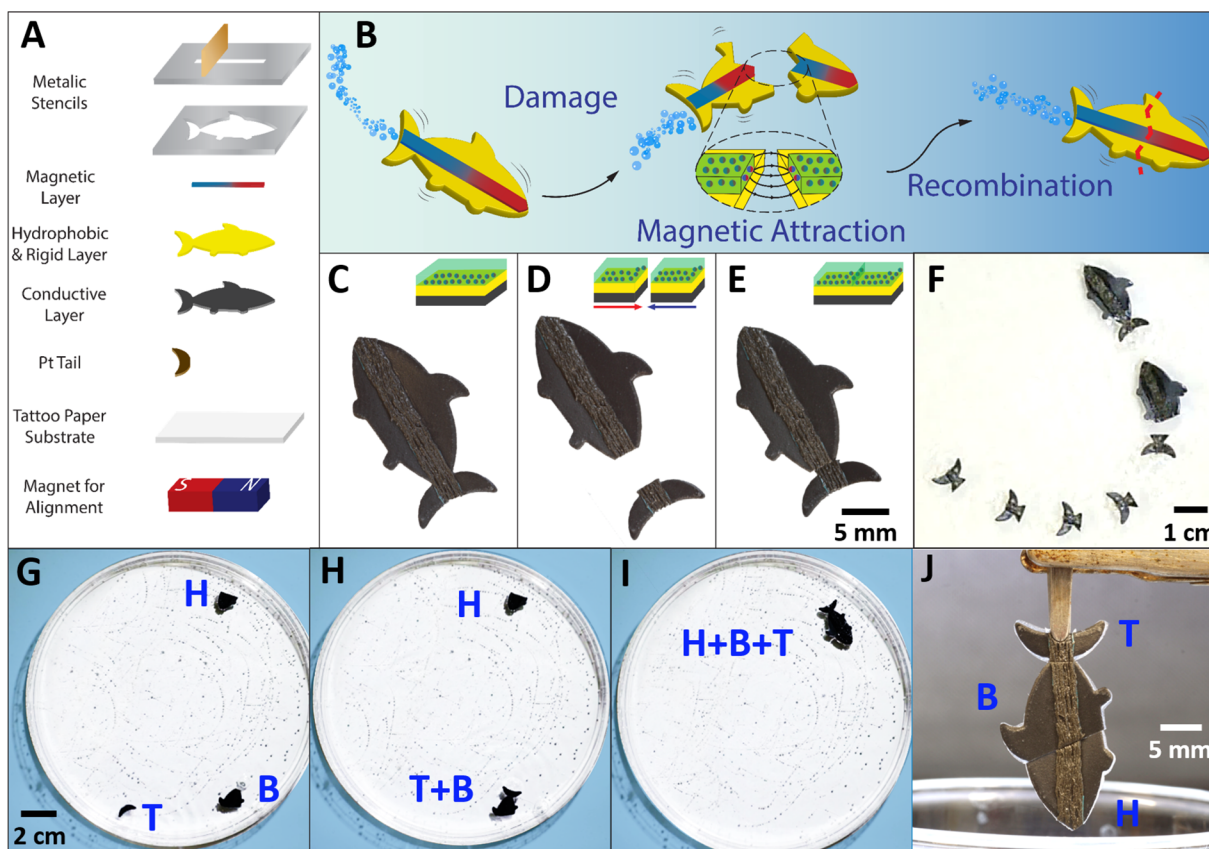
Figure 1. Autonomous "on-the-fly" self-healing of a magnetic based SHS. (A) Fabrication process of a SHS. (B) Diagram of a swimmer propelling in solution, experiencing extensive damage, and self-healing based on magnetic attraction. (C) Time-lapse images of a damaged swimmer healing over the course of 1.6 s. taken from Video S1. (D) Image of a pristine SHS on a dry surface. (E) Image of a swimmer damaged at the tail. (F) Image of the healed swimmer. (G) Images of a SHS damaged into three distinct pieces: head, (H), body (B), and tail (T). (H) Image of the healed tail and body. (I) Image of the completely healed swimmer. Taken from Videos S1. (J) Image of a healed swimmer suspended vertically while maintaining its integrity.

Herein, we present an autonomous "on-the-fly" recombination approach for small-scale chemically powered swimmers utilizing micro- and nanotechnology methods featuring the embedding of micro- and nanoparticles in a variety of polymer layers. Our swimmers are autonomously propelled, highlighting their unique ability to repair while in motion without aid from human operators. Movement is achieved by the catalytic decomposition of a peroxide fuel at the catalytic platinum (Pt) surface that generates an oxygen bubble thrust.[19−21] Due to the asymmetrical nature of our swimmer we see a mixture of linear and rotational motion which aids in covering a large area and aids in recombination. The self-healing swimmer (SHS) utilizes strong magnetic interactions to recover its swimming function. The built-in magnetic torque aligns and attracts the damaged pieces without user input or additional external triggers. Magnetic properties are attractive for such healing behavior as they are not readily inhibited by environmental conditions. While magnetic self-healing strategies using iron-oxide particles have been developed before, they have not been applied to robotics or as a standalone self-healing mechanism but usually have been applied in connection to hydrogel or polymeric healing materials.[22,23] Our goal is to introduce autonomous self-healing capabilities to small-scale untethered self-propelled robots and to shed useful insights on how autonomous self-healing can occur in dynamically moving systems. It should be pointed out that compared to common self-healing of stationary materials, the

motion is shown here to greatly facilitate healing at large distances as it brings the separated parts closer. The incorporation of strongly magnetic $Nd_2Fe_{14}B$ microparticles has been reported as an effective strategy to heal printed electronic devices.[24] The self-healing magnetic layer is incorporated in the form of a strip, or several strips, within the main body of the catalytic swimmer. In this work we investigate the importance of the alignment of the magnetic particles responsible for recombination of damaged pieces, assess the behavior of the swimmers before and after healing, and evaluate the healing efficiency of different magnetic healing strip designs and different cut positions with the goal of establishing some design parameters and evaluating the practicality of such a magnetic based self-healing strategy.

■ RESULTS

Fabrication and Operation of SHSs. The fabrication process is presented in Figure 1A. The main structure of the SHS features 3 layers: the conductive bottom layer, the rigid and hydrophobic middle layer and the top magnetic layer. Detailed information regarding the fabrication process is provided in the Supporting Information. After fabrication and release from the substrate, the SHSs are endowed with a catalytic propulsion capability by electrodeposition of Pt on their tail section for which the conductive bottom layer is necessary. The rigid hydrophobic middle layer is utilized to
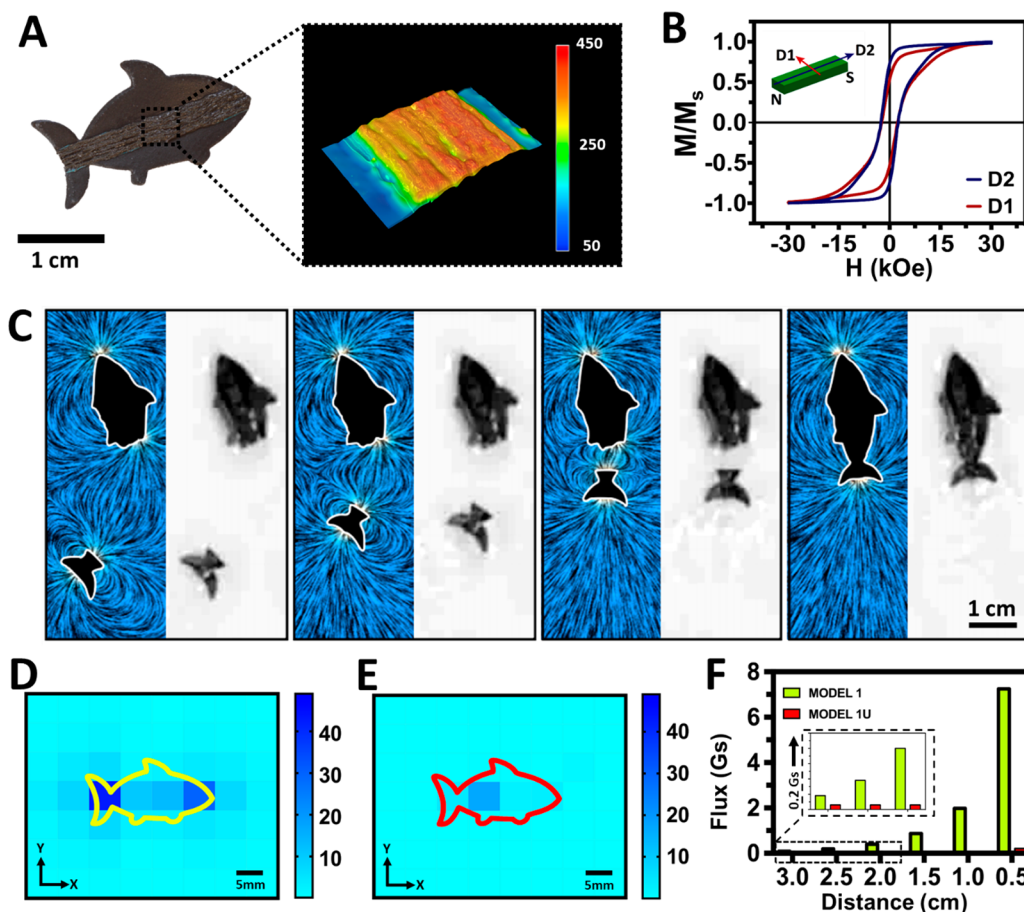
Figure 2. Assessment of the magnetic behavior of SHSs. (A) Image of a model 1 SHS. Inset represents topographical image of the magnetic strip of the SHS. Heat map is in μm. (B) Magnetic hysteresis loop of a magnetic strip perpendicular (D1, red) and parallel to the alignment axis (D2, blue). (C) Representation of the magnetic field around a SHS during a healing event. Taken from Video S2. (D) Grid of magnetic field measurement around a model 1 SHS. Heat map is in Gauss. (E) Grid of magnetic field measurement around a model 1U SHS. Heat map is in Gauss. (F) Magnetic flux as a function of separation distance for model 1 and model 1U SHSs. Inset shows a magnification of the region from 3 to 2 cm.

ensure strong swimming. The top magnetic strips enable the self-recombination following structural damage.

A schematic of the self-healing process of a typical swimmer is shown in Figure 1B. Initially, a pristine (nondamaged) SHS swims autonomously until it is damaged (separated into multiple pieces simulating brittle fracture due to the rigid and brittle nature of the conductive and hydrophilic layers). As the self-propelling tail portion of the SHS travels around, it is attracted to the static body piece (upon approaching it) due to the strong magnetic interactions of the magnetic strips until recombination occurs. The self-healed swimmer then restores the swimming in a manner similar to the pristine SHS. The proposed mechanism is first shown outside of the solution (no motion) with a model 1 SHS (1 magnetic stripe through the middle). Figure 1C shows the nondamaged swimmer. Next, the tail is detached from the body (Figure 1D). Finally, the tail reattaches to its body confirming the strong magnetic attraction. The healed SHS is shown in Figure 1E. The time-lapse images of Figure 1F (Video S1) show a damaged SHS, illustrating the reorientation and reattachment of the moving tail to its complementary static piece. At a large enough separation, the swimmer pieces do not feel each other as the magnetic attractive force is distance dependent. However, as the tail gets closer, the attractive magnetic force realigns the pieces so that the built-in movement brings them together and repair can occur autonomously. Since the magnetic force falls

off rapidly with distance it can only bring and align damaged portions of the SHS at distances around 50 mm. Hence, increasing vessel size increases the time for healing to occur. The versatility of the healing strategy is shown in Figure 1G where a SHS is cut into 3 pieces, named T, B, and H for tail, body, and head, respectively (Video S1). Additionally, the cut between the B and H sections was done at an oblique angle to test the versatility of the healing process. Following swimming of the T section for a few seconds it was attracted and reattached to the B, whereby the combined T+B structure restored its motion (Figure 1H). As this T+B portion continued its movement, it was attracted to the remaining H, resulting in complete recovery of the original SHS structure which continued to swim like the original pristine SHS (Figure 1I). Finally, to showcase the strength of the healing process, the recovered swimmer is hung vertically in Figure 1J, demonstrating that the magnetic force can hold the 3 pieces together against the forces of gravity.

Characterization of the Magnetic Behavior of SHSs. A typical model 1 swimmer with a focus on the magnetic strip is shown in Figure 2A. The topography of the strip was assessed via 3D light microscopy. The magnetic strip is printed in the presence of a strong external magnetic field in order to align the magnetic particles. The parallel grooves seen in the topographical image reconstruction attest to the alignment of the constituent magnetic particles.
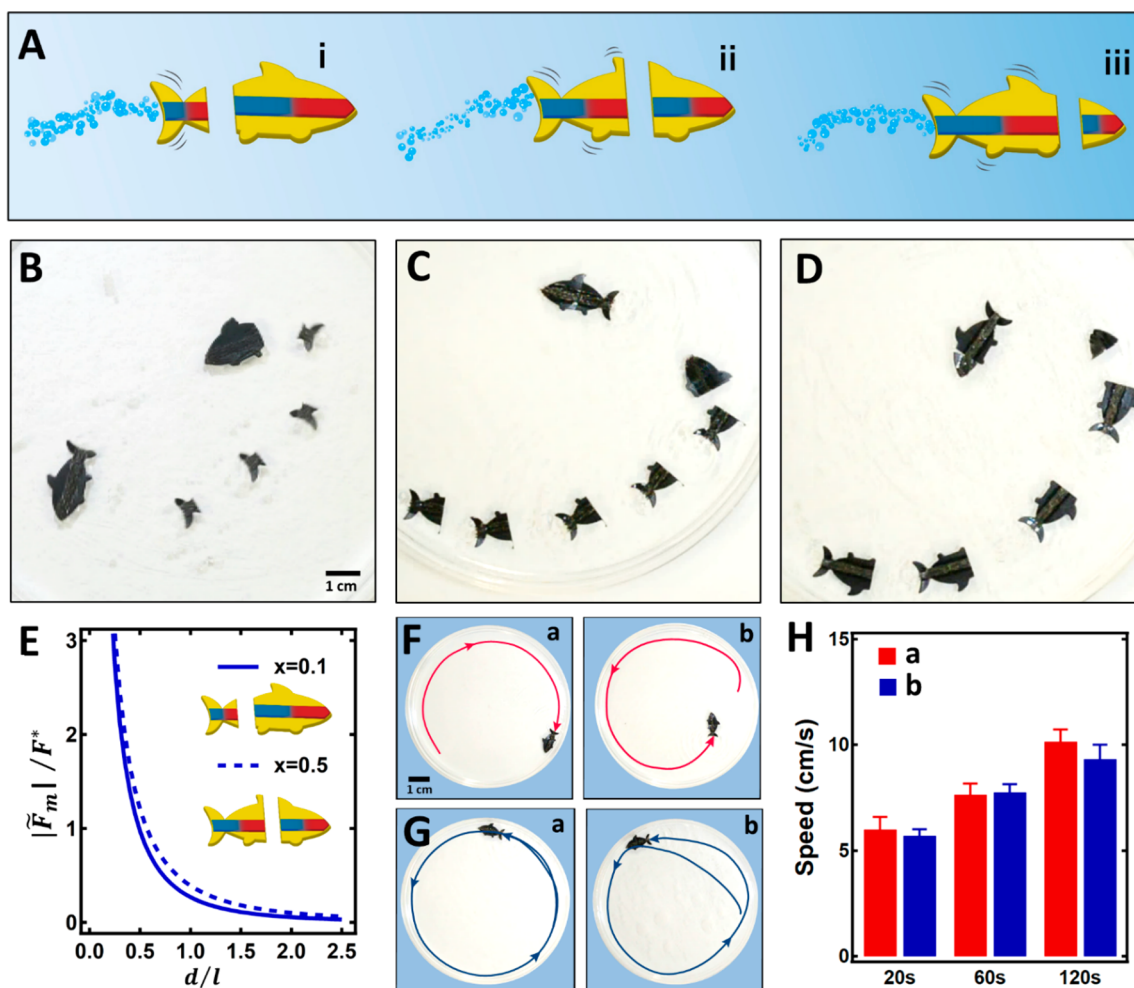
Figure 3. Influence of the damage position upon the propulsion behavior. (A) Diagram of some possible damage positions along the SHS: damage close to the tail (case i), halfway through the structure (case ii), and close to the head (case iii). (B, C, D) Time-lapse image of a model 1 SHS pertaining to cases i, ii, and iii, respectively. Taken from Video S4. (E) Plot of the normalized magnetic force as a function of the dimensionless separation distance for two different cut positions ($x = 0.1$ and 0.5) from an analytical model. (F) Propulsion of a pristine (a) and healed (b) SHS with 20 s deposited Pt on the tail. Trajectory shows motion over a 4 s period. (G) Propulsion of a pristine (a) and healed (b) SHS with a 120 s Pt deposition on the tail. The trajectory shows the motion over a 4 s duration. (H) Effect of the Pt deposition time upon the speed of pristine (red) and healed (blue) SHSs.

Next, the magnetic strip was subjected to a magnetic hysteresis test to quantitatively assess the alignment of the magnetic dipoles within the strip. The normalized (M/M_s) hysteresis loops (Figure 2B) show typical hard magnetic behavior, with high magnetic remanence (M_r) and magnetic coercivity, H_c. The magnetic saturation (M_s) of the strip was ~87 emu/g, along with a magnetic coercivity, H_c, of ~2.5 kOe and a highest M_r value of 61.48 emu/g. Importantly, the curves reveal clear alignment of the magnetic particles in the SHSs. The red trace (D1, alignment perpendicular to the magnetic field) has a M_r/M_s ratio of 0.53 while the blue trace (D2, alignment parallel to the magnetic field) exhibits a M_r/M_s of 0.74. Typically, in well-aligned samples, there is a clear directional dependence of the magnetic properties, reminiscent of highly anisotropic magnetic materials.[25,26] A $M_r/M_s \sim 0.5$ is typical of randomly oriented material while a high ($M_r/M_s > 0.5$) value is indicative of well aligned magnetic material. The high M_r/M_s ratio (0.74) in the D2 direction clearly shows that the magnetic particles are well aligned along the long axis of the strip.

Analysis of Video S2 provides a direct representation of the magnetic field around a swimmer or parts of a swimmer (Figure 2C), with further details found in the Supporting Information. Based on the orientation of the magnetic field lines it is clear that model 1 SHS magnetic strips acts as dipole permanent magnets even when separated. As the mobile tail approaches the static swimmer piece, the magnetic fields overlap until the self-healing process restores the initial structure. Finally, the overlap of the magnetic fields produces only one magnetic dipole, confirming the structural integrity of the swimmer.

Next, the magnetic field strength was verified with a handheld Gauss meter. The heat map grid of Figure 2D illustrates the concentration of magnetic flux along the body and surroundings of a model 1 SHS whose strip has been aligned with a strong magnetic field. Due to the magnetic alignment the SHS exhibits stronger field values compared to an unaligned SHS (model 1U) (Figure 2E). Note that the highest field values are recorded at the head and tail of the swimmer, affirming that the dispersion of magnetic particles and the alignment make the strip act as a bar magnet. Figure
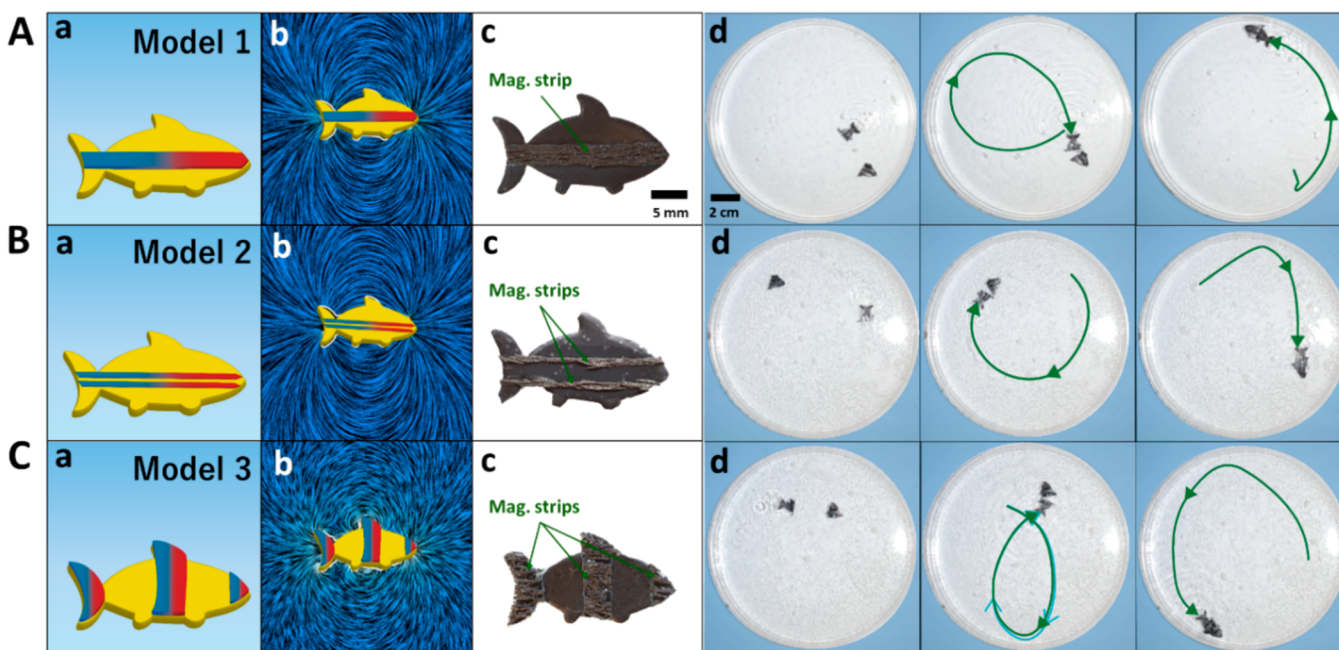
Figure 4. Healing behavior of different magnetic strip configurations. (A) Model 1 SHS: schematic (a), visual representation of the magnetic field lines (b), zoom-in image (c), and images of damaged, approaching and healed states (d). (B) Model 2 SHS: schematic (a), visual representation of the magnetic field lines (b), zoom-in image (c), and images of damaged, approaching and healed states (d). (C) Model 3 SHS: schematic (a), visual representation of the magnetic field lines (b), zoom-in image (c), and images of damaged, approaching and healed states (d). Taken from Video S5.

2F illustrates how the magnetic flux diminishes with distance for model 1 and 1U swimmers. The former displays strong magnetic flux at larger distances, realized by aligning the particles during fabrication. This was also verified by a model 1U swimmer in solution (Figure S1, Video S3). Despite the approach of the active tail to the passive piece and the physical contact of the 2 pieces, there is no lasting attraction and hence no structural recovery, confirming the crucial importance of magnetic alignment during fabrication.

Effect of the Damage Position on Healing Behavior and Efficiency. Next, we investigated the self-healing capabilities as a function of the damage location using model 1 SHSs. We studied three different cases (Figure 3A). Case i features a cut 7 mm away from the tail end of the swimmer. Case ii features a cut exactly in the middle of the swimmer, while case iii corresponds to damage 6 mm away from the front of the SHS. Additionally, to evaluate the healing effectiveness of the model 1 SHS based on the damage position, we define a healing efficiency (HE) as the number of times the swimmer has successfully and autonomously healed, retaining both the pristine structure and initial propulsion, divided by all of the reattachment events

$$\left(HE = \frac{\text{Healing events with recovered propulsion and correct structure}}{\text{All recombination events}} \times 100\% \right) \tag{1}$$

We can go further and calculate the overall healing efficiency (OHE) which also takes into account the cases when the healing is imperfect (mismatching), while the swimmer retains the propulsion capability

$$\left(OHE = \frac{\text{Healing events with recovered propulsion and mismatched structure}}{\text{All recombination events}} \times 100\% \right) \tag{2}$$

Finally, the remaining healing events feature a reattachment with large structural mismatch and loss of the autonomous motion (SHS is spinning or stuck on the wall). A real example of case i SHS is demonstrated in Figure 3B. In this case, the passive body is large relative to the mobile tail and does not rotate to match the self-propelling tail because of its size and weight. On the other hand, the tail moves rapidly, fixing itself to the body and reattaching easily. Case i exhibits a HE of 88% with an OHE of 94%. For case ii, both pieces exhibit some rotation and alignment as their respective sizes are very similar (Figure 3C). Case ii demonstrates a HE and OHE of 86%, demonstrating that the size of the passive and active portions of the swimmer affects the healing process. In case iii, the smaller head has a higher propensity to change its direction and align to the magnetic field of the larger propelling tail-containing body (Figure 3D). Yet, at the same time the propulsion force of the catalytic propulsion overcomes the magnetic force, affecting the healing capability of the body, leading to diminished healing capability, indicated by a HE of 58% and OHE of 71%. Furthermore, we compared these results with predictions of the magnetic force between the magnetic strips of a damaged swimmer from an analytical model (Figure 3E). As expected, the force falls off rapidly with separation distance. More interestingly, the magnetic force depends on the position of the cut (denoted by x). With smaller x (larger size difference between the two damaged pieces) the force is smaller, suggesting lower healing ability.

To investigate this further, we performed simulations of the magnetic torque of the swimmers in many orientations and distances away from each other (Figure S3). A more detailed

explanation is provided in the Supporting Information. Overall, the data of Figure S3 suggest that the magnetic torque will most likely align damaged pieces at all orientations at short distances while at large distances the orientations which will lead to healing become more restricted.

SHSs with different speeds were prepared by electroplating different amounts of Pt (using 20 or 120 s deposition; 60 s used in all other experiments). Figure 3F presents an SHS with 20 s Pt deposited tail. The trajectory exhibits the motion of the pristine (a) and healed (b) cases over a 4 s period, illustrating a very similar propulsion behavior after healing. For the faster swimmer (based on the 120 s Pt plating), the pristine (a) and healed (b) trajectories show little variation (Figure 3G). A very small difference between the speed of the pristine and healed swimmers is observed for these different catalytic swimmers, with the speed of healed swimmers being slightly lower compared to the pristine ones (Figure 3H; a vs b). Thus, while longer Pt deposition times increase swimmer speed, there does not seem to be an effect on the propulsion behavior of the swimmer after healing.

Effect of the Magnetic Strip Configuration on Healing Behavior and Efficiency. Assessing the healing behavior of different magnetic configurations is an important step toward optimizing the healing process. Figure 4A showcases the schematic (a) of a model 1 SHS. Additionally, we provide a visual representation of the magnetic field lines around each swimmer to aid in understanding the healing behavior (b) and an image of the swimmer (c) with zoom-in images in Figure S4. For model 1 (damaged in the middle) the propelling tail easily finds its complementary passive section, reattaches, and with the healed swimmer continues to move similar to the pristine version (c) (Video S5). A similar behavior is observed for the two-strip (model 2) swimmer (Figure 4B, Video S5). Compared to model 1, a model 2 SHS demonstrates a HE of 49% and OHE of 69%. Thus, the two-strip configuration is not as effective as model 1. The larger difference between the HE and OHE indicates that there is a large number of imperfect healing events. This can be attributed to the larger surface that multiple strips cover. Using the same magnetic alignment, model 3 SHS also presented effective healing after being damaged in the middle (Figure 4C, Video S5), exhibiting a HE of 41% and OHE of 63%. For model 3, the magnetic healing surface is spread out over a larger area preventing accurate healing but still retaining a high percentage of imperfect healing events. At the same time, the large area of magnetically active material may cause the attachment of passive pieces to multiple areas of the swimmer besides the specific damaged area. This is supported by the representation of the magnetic field around the swimmer models 2 and 3 (b). Figure S5 presents several examples of imperfect healing (top row: imperfect healing considered for OHE; bottom row: unsuccessful healing). For example, SHSs can exhibit reattachment that is offset or imperfect, noticed particularly for models 2 and 3, owing to the larger area of active magnetic material along the cut. Another improper healing even occurs when the damaged pieces heal in an incorrect order, such as the cases for models 1 and 2. In these examples, the propelling tail may randomly reattach first to the head (instead of the body) resulting in undesirable configurations.

The present work demonstrates the first example of a functional small swimmer, capable of responding to damage and restoring its structure autonomously and "on-the-fly". To achieve this goal, we introduce the concept of autonomous self-healing to such self-propelled robots and obtain useful insights on how such a healing process occurs in dynamically moving systems.. The SHSs are easy to fabricate without resorting to complex synthetic efforts and offer many benefits for future endeavors. Simply by printing the desired structure and aligning magnetic $Nd_2Fe_{14}B$ particles in the desired dipole direction imparts high verstatility toward utilizing a variety of designs (i.e., Models 1, 2, and 3). These include robust and facile healing and the ability to self-repair repeatedly in the same location in the absence of external stimuli or user input. While the presented swimmer moves on the surface of water, we believe this concept can be applied to 3D swimmers moving in bulk fluids. While catastrophic damage was used here to demonstrate the new healing concept, such an approach can be applied to a variety of common situations involving compromise of the swimmer structure.

One of the main applications for these small-scale swimmers is in remediation or industrial clean up. For example, introducing functionalized swimmers as sponges to sequester heavy metals, purify water, or decompose organics or nerve agents will increase the process's efficiency due to their movement. Many of these applications rely on hydrogen peroxide, making these peroxide-powered swimmers an easy addition. Due to the multicomponent nature of these processes, additional studies need to be performed on the propulsion and healing within environments with different viscosities, temperatures, and chemical makeup compared to the one used in this study.

Despite these distinct advantages and potential benefits, several challenges must be addressed before further practical use. For example, the healing process is still prone to imperfect healing events. It is necessary for programmable and intelligent self-healing strategies which bypass misaligned or out-of-order recombination to be developed. We envision that adding more complexity to these swimming platforms, e.g., by incorporating stimuli-responsive materials, will add a basic feedback capability and impart adaptability to their surrounding environment. As seen above, the magnetic interaction can be weak over large distances, hindering the healing in large reservoirs and requiring strategies for actively directing swimmers toward a target location or preconcentrating them. In order to demonstrate that our swimmers can handle a variety of environments, we also envision introducing them into larger swimming pools (i.e., > 10× the size of the swimmer) and pools with corners (i.e., 90° or >90°). Next comes the issue of multiple swimmers attempting to heal and producing mismatched assemblies. To alleviate this, we envision structures resembling our Model 2 swimmer where adjacent strips (2 or more) will have a preset pattern of dipole direction orientation to produce unique configurations to reduce the chance of healing with noncomplementary pieces. Furthermore, the mismatched healed configurations represent a low energy situation due to the attraction of the magnets but not necessarily the lowest energy configuration. To attain this configuration (i.e., correct healing) some annealing strategies are envisioned whether due to fluid dynamics, additional magnetic stimuli, or others.[27,28] Another way to control the magnetic response would be by adding paramagnetic materials, instead of ferromagnetic ones, in order to turn on/off the magnetic capabilities of the swimmer and choose when to initiate or dissociate healing. However, this strategy would require application of an external magnetic field. Scaling the

swimmer up or down provides additional challenges where the size of the magnetic portion has to be scaled accordingly with the body. Furthermore, the speed of the swimmer must match the size of the container to provide self-recombination at reasonable time scales. Conversely, shrinking the swimmer or utilizing microsized self-propelled structures (e.g., Janus micromotors or tubular microrockets) does not make as much sense in terms of self-healing because inertia plays a much smaller role at the microscale and catastrophic failure usually results from micromotors getting stuck rather than breaking apart. Additionally, nontoxic fuels must be developed to replace the peroxide fuel used in this proof-of-concept study.

■ ASSOCIATED CONTENT

ⓈⒾ Supporting Information

The Supporting Information is available free of charge at https://pubs.acs.org/doi/10.1021/acs.nanolett.0c05061.

> Materials and Methods section, images of unsuccessful healing of model 1U SHS, flow pattern around a SHS, explanation of the magnetic interaction model used in Figure 3, simulation of the magnetic torque between two parts of an SHS in different orientations and positions, images of self-healed models 1, 2, and 3, images of misaligned healing (PDF)
>
> Video of self-healing swimmers (AVI)
>
> Video of the magnetic field distribution during self-healing (AVI)
>
> Video of unsuccessful healing of a model 1U swimmer (AVI)
>
> Video of the effect of cut position on self-healing (AVI)
>
> Video of the effect of strip geometry on self-healing (AVI)

■ AUTHOR INFORMATION

Corresponding Author

Joseph Wang − *Department of NanoEngineering, University of California San Diego, La Jolla, California 92093, United States;* ⓘ orcid.org/0000-0002-4921-9674; Email: josephwang@eng.ucsd.edu

Authors

Emil Karshalev − *Department of NanoEngineering, University of California San Diego, La Jolla, California 92093, United States*

Cristian Silva-Lopez − *Department of NanoEngineering, University of California San Diego, La Jolla, California 92093, United States*

Kyle Chan − *Department of Mechanical and Aerospace Engineering, University of California San Diego, La Jolla, California 92093, United States*

Jieming Yan − *Department of NanoEngineering, University of California San Diego, La Jolla, California 92093, United States*

Elodie Sandraz − *Department of NanoEngineering, University of California San Diego, La Jolla, California 92093, United States*

Mathieu Gallot − *Department of NanoEngineering, University of California San Diego, La Jolla, California 92093, United States*

Amir Nourhani − *Department of NanoEngineering, University of California San Diego, La Jolla, California 92093, United States;* ⓘ orcid.org/0000-0002-7951-9483

Javier Garay − *Department of Mechanical and Aerospace Engineering, University of California San Diego, La Jolla, California 92093, United States*

Complete contact information is available at:
https://pubs.acs.org/10.1021/acs.nanolett.0c05061

Author Contributions

§E.K. and C.S.-L. contributed equally to this work.E.K., C.S. and J.W. conceived the idea and designed the experiments. E.K., C.S., J.Y., and E.S. performed all of the experiments. K.C. performed the magnetic hysteresis measurements. M.G. and A.N. performed the magnetic field, force and torque simulations and modeling, respectively. All authors assisted in data analysis and the manuscript preparation. Additionally, the authors thank Xiaolong Lu for fruitful discussions. The authors acknowledge Fernando Soto for assisting with the 3D light microscopy.

Notes

The authors declare no competing financial interest.

■ ACKNOWLEDGMENTS

■ REFERENCES

(1) Wang, J. *Nanomachines: Fundamentals and Applications*; John Wiley & Sons, Inc.: Weinheim, Germany, 2013.

(2) Karshalev, E.; Esteban-Fernández de Ávila, B.; Wang, J. Micromotors for "Chemistry-on-the-Fly. *J. Am. Chem. Soc.* **2018**, *140*, 3810−3820.

(3) Hines, L.; Petersen, K.; Lum, G. Z.; Sitti, M. Soft Actuators for Small-Scale Robotics. *Adv. Mater.* **2017**, *29*, 1603483.

(4) Hu, W.; Lum, G. Z.; Mastrangeli, M.; Sitti, M. Small-Scale Soft-Bodied Robot With Multimodal Locomotion. *Nature* **2018**, *554*, 81−85.

(5) Zhu, W.; Li, J.; Leong, Y. J.; Rozen, I.; Qu, X.; Dong, R.; Wu, Z.; Gao, W.; Chung, P. H.; Wang, J.; Chen, S. 3D-Printed Artificial Microfish. *Adv. Mater.* **2015**, *27*, 4411−4417.

(6) Karshalev, E.; Kumar, R.; Jeerapan, I.; Castillo, R.; Campos, I.; Wang, J. Multistimuli-Responsive Camouflage Swimmers. *Chem. Mater.* **2018**, *30*, 1593−1601.

(7) Esteban-Fernández de Ávila, B.; Angsantikul, P.; Li, J.; Lopez-Ramirez, M. A.; Ramírez-Herrera, D. E.; Thamphiwatana, S.; Chen, C.; Delezuk, J.; Samakapiruk, R.; Ramez, V.; Obonyo, M.; Zhang, L.; Wang, J. Micromotor-Enabled Active Drug Delivery For In Vivo Treatment Of Stomach Infection. *Nat. Commun.* **2017**, *8*, 272.

(8) Rich, S. I.; Wood, R. J.; Majidi, C. Untethered Soft Robotics. *Nat. Electron.* **2018**, *1*, 102−112.

(9) Terryn, S.; Brancart, J.; Lefeber, D.; Assche, G. V.; Vanderbroght, B. Self-Healing Soft Pneumatic Robots. *Sci. Robot.* **2017**, *2*, No. eaan4268.

(10) Cao, J.; Zhou, C.; Su, G.; Zhang, X.; Zhou, T.; Zhou, Z.; Yang, Y. Arbitrarily 3D Configurable Hygroscopic Robots with A Covalent-Noncovalent Interpenetrating Network And Self-Healing Ability. *Adv. Mater.* **2019**, *31*, 1900042.

(11) Shepherd, R. F.; Stokes, A. A.; Nunes, R. M. D.; Whitesides, G. M. Soft Machines That Are Resistant To Puncture And That Self Seal. *Adv. Mater.* **2013**, *25*, 6709−6713.

(12) Kazem, N.; Bartlett, M. D.; Majidi, C. Extreme Toughening Of Soft Materials With Liquid Metal. *Adv. Mater.* **2018**, *30*, 1706594.

(13) Markvicka, E. J.; Bartlett, M. D.; Huang, X.; Majidi, C. An Autonomously Electrically Self-Healing Liquid Metal-Elastomer

Composite For Robust Soft-Matter Robotics and Electronics. *Nat. Mater.* **2018**, *17*, 618−624.

(14) Acome, E.; Mitchell, S. K.; Morrissey, T. G.; Emmett, M. B.; Benjamin, C.; King, M.; Radakovitz, M.; Keplinger, C. *Science* **2018**, *359*, 61−65.

(15) Tolley, M.; Krishnan, M.; Erickson, D.; Lipson, H. *Appl. Phys. Lett.* **2008**, *93*, 254105.

(16) Diller, E.; Zhang, N.; Sitti, M. Modular Micro-Robotic Assembly Through Magnetic Actuation and Thermal Bonding. *J. Micro-Bio Robot.* **2013**, *8*, 121−131.

(17) Pawashe, C.; Diller, E.; Floyd, S.; Sitti, M. *Paper presented at the 2011 IEEE International Conference on Robotics and Automation*, Shanghai, China, May 2011.

(18) Sumerlin, B. S. Next-Generation Self-Healing Materials. *Science* **2018**, *362*, 150−151.

(19) Gao, W.; Sattayasamitsathit, S.; Orozco, J.; Wang, J. Highly Efficient Catalytic Microengines: Template Electrosynthesis Of Polyaniline/Platinum Microtubes. *J. Am. Chem. Soc.* **2011**, *133*, 11862−11864.

(20) Kumar, R.; Kiristi, M.; Soto, F.; Li, J.; Singh, V. V.; Wang, J. Self-Propelled Screen-Printable Catalytic Swimmers. *RSC Adv.* **2015**, *5*, 78986−78993.

(21) Ismagilov, R. F.; Schwartz, A.; Bowden, N.; Whitesides, G. M. Autonomous Movement and Self-Assembly. *Angew. Chem., Int. Ed.* **2002**, *41*, 652−624.

(22) Zhang, Y.; Yang, B.; Zhang, X.; Xu, L.; Tao, L.; Li, S.; Wei, Y. A Magnetic Self-Healing Hydrogel. *Chem. Commun.* **2012**, *48*, 9305−9307.

(23) Huang, Y.; Huang, Y.; Zhu, M.; Meng, W.; Pei, Z.; Liu, C.; Hu, H.; Zhi, C. Magnetic-Assisted, Self-Healable, Yarn-Based Super-capacitor. *ACS Nano* **2015**, *9*, 6242−6251.

(24) Bandodkar, A. J.; López, C. S.; Mohan, A. M. V.; Yin, L.; Kumar, R.; Wang, J. All-Printed Magnetically Self-Healing Electro-chemical Devices. *Sci. Adv.* **2016**, *2*, No. e1601465.

(25) Pullar, R. C.; Bhattacharya, A. K. The Magnetic Properties of Aligned M Hexa-Ferrite Fibres. *J. Magn. Magn. Mater.* **2006**, *300*, 490−499.

(26) Volodchenkov, A. D.; Ramirez, S.; Samnakay, R.; Salgado, R.; Kodera, Y.; Balandin, A. A.; Garay, J. E. Magnetic And Thermal Transport Properties Of $SrFe_{12}O_{19}$ Permanent Magnets With Anisotropic Grain Structure. *Mater. Des.* **2017**, *125*, 62−68.

(27) Mermoud, G.; Mastrangeli, M.; Upadhyay, U.; Martinoli, A. Real-Time Automated Modeling and Control of Self-Assembling Systems. Conference paper in *Proceedings − IEEE International Conference on Robotics and Automation*; 2012.

(28) Haghighat, B.; Mastrangeli, M.; Mermoud, G.; Schill, F.; Martinoli, A. Fluid-Mediated Stochastic Self-Assembly at Centimetric and Sub-Millimetric Scales: Design, Modeling, and Control. *Micro-machines* **2016**, *7*, 138−161.